

Article

IMODBO for Optimal Dynamic Reconfiguration in Active Distribution Networks

Naiwei Tu and Zuhao Fan * 

Faculty of Electrical and Control Engineering, Liaoning Technical University, Huludao 125105, China

* Correspondence: fzh5653150@163.com

Abstract: A dynamic reconfiguration method based on the improved multi-objective dung beetle optimizer (IMODBO) is proposed to reduce the operating cost of the distribution network with distributed generation (DG) and ensure the quality of the power supply, while also minimizing the number of switch operations during dynamic reconfiguration. First, a multi-objective model of distribution network dynamic reconfiguration with the optimization goal of minimizing active power loss and voltage deviation is established. Secondly, the K-means++ clustering algorithm is used to divide the daily load of the distribution network into periods. Finally, using the IMODBO algorithm, the distribution network is reconstructed into a single period. The IMODBO algorithm uses the chaotic tent map to initialize the population, which increases the ergodicity of the initial population and solves the problem of insufficient search space. The algorithm introduces an adaptive weight factor to solve the problem of the algorithm easily falling into a locally optimal solution in the early stage with weak searchability in the later stage. Levy flight is introduced in the perturbation strategy, and a variable spiral search strategy improves the search range and convergence accuracy of the dung beetle optimizer. Reconfiguration experiments on the proposed method were conducted using a standard distribution network system with distributed power generation. Multiple sets of comparative experiments were carried out on the IEEE 33-nodes and PG&E 69-nodes. The results demonstrated the effectiveness of the proposed method in addressing the multi-objective distribution network dynamic reconfiguration problem.

Keywords: IMODBO; K-means++; network reconfiguration; renewable energy sources; voltage fluctuations



Citation: Tu, N.; Fan, Z. IMODBO for Optimal Dynamic Reconfiguration in Active Distribution Networks.

Processes **2023**, *11*, 1827. <https://doi.org/10.3390/pr11061827>

Academic Editors: Victor M. Becerra and Ahmed Rachid

Received: 20 May 2023

Revised: 11 June 2023

Accepted: 13 June 2023

Published: 15 June 2023



Copyright: © 2023 by the authors. Licensee MDPI, Basel, Switzerland. This article is an open access article distributed under the terms and conditions of the Creative Commons Attribution (CC BY) license (<https://creativecommons.org/licenses/by/4.0/>).

1. Introduction

1.1. Motivation

The prevalence of low-carbon power system networks is a trend that conforms to the development of new energy technologies. Such systems also represent a meaningful way to promote the high-quality development of clean energy [1–3]. Owing to the accessibility of distributed renewable energy [4], instability is associated with a number of non-traditional safety problems in the stable operation of the distribution network systems. By manipulating section switches and tie switches, distribution network reconfiguration can alter the network topology and optimize power transmission within the distribution network system.

1.2. Literature Review

Domestic and foreign scholars have been devoted to researching algorithms to solve the distribution network reconfiguration problem. Existing algorithms are classified into three categories: traditional mathematical optimization algorithms [5,6], heuristic algorithms [7,8], and intelligent optimization algorithms [9–11]. A reconfiguration model needs to be established for the distribution network before solving the problem using traditional mathematical optimization algorithms that only solve single-objective models. Given the increasing complexity of distribution network systems in recent years, the data involved in the distribution

network have become more extensive, resulting in long computing times and difficulty in solving the distribution network reconfiguration problem. Heuristic algorithms establish some effective rules to solve the distribution network reconfiguration problem by analyzing the situation. These algorithms include branch exchange algorithms, optimal flow algorithms, etc. However, the optimization abilities of heuristic algorithms are poor.

Various optimization methods have been proposed to solve the distribution network reconfiguration problem. Li et al. [12] proposed a dynamic reconfiguration integrated optimization method based on a multi-objective sparrow search algorithm, optimizing multiple objectives, including power quality, economic efficiency, and energy loss, and comparing various algorithms, has achieved good results. Wang et al. [13] proposed a distribution network reconfiguration method that considers the network's reliability, economy, and environmental friendliness based on a parallel slime mold algorithm. When solving multi-objective optimization problems, using a weighted method to transform multiple objectives into a single objective may result in the inability to obtain the actual optimal value in a complex system. This is because the weights are preset. Gao et al. [14] proposed a multi-objective optimization method that effectively finds the optimal energy configuration scheme for intelligent communities using Levy flight and an improved chicken swarm algorithm, which enhances the algorithm's global and local search abilities. In addition, a comprehensive set of scenario simulations was conducted to test the model. The results demonstrate that the improved algorithm effectively overcomes the issue of being trapped in local optima. Mahdad et al. [15] proposed an optimal reconfiguration and reactive power planning method based on a fractal search algorithm, which can simultaneously consider multiple indicators and has high search efficiency and optimization accuracy. Kefayat et al. [16] proposed a hybrid approach that combines ant colony optimization and an artificial bee colony algorithm to optimize the placement and sizing of distributed energy resources with probabilistic constraints. The system dynamically switches between the two algorithms through an adaptive strategy to achieve better optimization performance. Jafari et al. [17] proposed a parallel implementation of the exchange market algorithm (EMA) and wild goats algorithm (WGA), which improved the computational speed and accuracy. However, their study on distribution network systems did not consider the presence of distributed energy resources. Parizad et al. [18] proposed a novel algorithm based on particle swarm optimization (PSO) for distribution feeder reconfiguration (DFR). The algorithm aims to minimize short-circuit levels in power distribution systems and is validated using the IEEE 83 bus power distribution system model, demonstrating its effectiveness. These optimization methods demonstrate the diverse strategies used to solve distribution network reconfiguration problems, and each method has its strengths and limitations depending on the problem being addressed.

Numerous researchers have proposed intelligent optimization algorithms by analyzing the habits and physical phenomena of various biological populations. Algorithm technology is a continuously evolving field that undergoes frequent updates and iterations. In 2022, Jiankai Xue introduced a new swarm intelligence optimization algorithm called the dung beetle optimizer (DBO) [19]. The DBO algorithm employs multiple search strategies and can perform local and global searches, demonstrating a fast convergence speed and high solution accuracy. The DBO algorithm has vast potential for application in various fields. The development of this algorithm represents a significant contribution to the advancement of optimization algorithms.

1.3. Contributions

In this study, we propose a dynamic reconfiguration method for distributed generation and distribution networks using the improved multi-objective dung beetle optimizer (IMODBO). This method establishes a multi-objective model with active power loss and voltage deviation as objective functions. According to the characteristics of the problem, the K-means++ clustering algorithm is used to divide the daily load into periods, and the IMODBO algorithm is used to transform the single-period distribution network. The

IMODBO algorithm uses a tent chaotic map in the population initialization process to improve the quality and ergodicity of the initial population. The adaptive weight factor solves the problem of early convergence and weak searchability of the algorithm. Levy flight perturbation and variable spiral strategy enhance the global search ability of the algorithm. The validity of the proposed method was verified by a reconstruction experiment on the IEEE 33-node and the PG&E 69-node power distribution system. Against previous studies, the main contributions are summarized below.

- The dynamic distribution network model with distributed power generation was established, aiming to minimize the active power loss and voltage deviation.
- In response to the multi-objective optimization problem of distribution network re-configuration, a improved multi-objective dung beetle optimizer (IMODBO) is proposed. Compared with various state-of-the-art single-objective and multi-objective algorithms, IMODBO demonstrates superior convergence speed and exploration capability.
- The distribution network reconfiguration problem is solved using IMODBO combined with the K-means++ clustering algorithm. By comparing with existing algorithms and conducting multiple scenario tests on the IEEE 33-node and PG&E 69-node standard distribution network systems, significant improvements are achieved.
- The experimental results demonstrate that the proposed method effectively reduces active power losses, stabilizes node voltage distribution, and significantly reduces the number of reconfigurations required.

The organization of this study is as follows: Section 2 introduces the dynamic re-configuration optimization model for power distribution systems, including the constraints of distributed power generation. Section 3 presents the application of the K-means++ clustering algorithm, the improvement measures of IMODBO, and the optimization process for solving the distribution network. Section 4 validates the effectiveness of the improved algorithm through various test functions and verifies the proposed method in the different scenarios of two distribution network systems. Section 5 concludes the findings of this study, analyzes the limitations of the proposed method, and presents future research directions.

2. Problem Formulation

The proposed research methodology utilizes the IMODBO to optimize the active power loss and voltage deviation in distribution network systems. The algorithm is applied to determine the optimal configuration of the distribution network. The effectiveness of the proposed algorithm is validated using the IEEE 33-node system and the PG&E 69-node system.

2.1. Objective Function

To improve the transmission efficiency of the distribution network, the active network loss of the reconstructed distribution network is optimized to reduce the distribution network's power cost and enhance its reliability and stability. The minimum active power loss of the distribution network after reconstruction can be expressed as follows [20]:

$$F_1 = \min \sum_{t=1}^T \sum_{l=1}^G k_{t,l} R_l \frac{P_{t,l}^2 + Q_{t,l}^2}{U_{t,l}^2} \quad (1)$$

where T represents the reconfiguration interval; G represents the total number of branches in the distribution network system; $k_{t,l}$ represents the first state at the l -th branch during the t -th period, where $k_{t,l} = 1$ means that the l -th branch during the t -th period is closed, and $k_{t,l} = 0$ means that the l -th branch during the t -th period is disconnected; $P_{t,l}$ and $Q_{t,l}$ represent the active power and reactive power at the l -th branch during the t -th period, respectively; R_l is the resistance of the l -th branch; and $U_{t,l}$ represents the node voltage at the end of the l -th branch during the t -th period.

A voltage offset model of the system is established to balance the voltage distribution of each node in the distribution network. Reducing the voltage offset can improve the stability and reliability of the distribution network, reduce energy waste, and reduce the incidence of equipment failure. The minimum voltage deviation of the distribution network after reconfiguration can be expressed as [21]

$$F_2 = \min \sum_{t=1}^T \sum_{i=1}^N \frac{|U_{t,i} - U_{t,i}^*|}{U_i^*} \quad (2)$$

where $U_{t,i}$ represents the actual voltage value at the i -th node during the t -th period, N represents the total number of nodes in the model, and U_i^* represents the rated voltage of the i -th node.

2.2. Constraint Conditions

In order to demonstrate the feasibility of the reconfiguration, the process must adhere to certain constraints, including power flow, nodal voltage, branch current, and distributed generation power.

(1) Equality constraint of the power flow equation [22]

$$\begin{cases} P_{t,i} + P_{t,DGi} = P_{t,loadi} + U_{t,i} \sum_{j=1}^N U_{t,j} (G_{ij} \cos \delta_{t,ij} + B_{ij} \sin \delta_{t,ij}) \\ Q_{t,i} + Q_{t,DGi} = Q_{t,loadi} + U_{t,i} \sum_{j=1}^N U_{t,j} (G_{ij} \sin \delta_{t,ij} - B_{ij} \cos \delta_{t,ij}) \end{cases} \quad (3)$$

where i and j represent the start and end nodes of the branch, respectively; $P_{t,i}$, $P_{t,DGi}$, and $P_{t,loadi}$ represent the power injected into the network, the distributed power output, and the active power at the i -th node during the t -th period, respectively; $Q_{t,i}$, $Q_{t,DGi}$, and $Q_{t,loadi}$ represent the network injected power, distributed power output, and reactive power at the i -th node during the t -th period, respectively; $U_{t,i}$ and $U_{t,j}$ represent the voltage of the i -th and j -th node during the t -th period, respectively; and $\delta_{t,ij}$, G_{ij} , and B_{ij} represent the phase angle difference, susceptance, and conductance between nodes i, j , respectively.

(2) Node voltage constraint [23]

$$U_{i,\min} \leq U_{t,i} \leq U_{i,\max} \quad (4)$$

where $U_{i,\min}$ and $U_{i,\max}$ represent the lower and upper limits of the allowable voltage at the i -th node, respectively, and U_i^{\min} and U_i^{\max} take $0.9U_{t,i}$ and $1.05U_{t,i}$, respectively.

(3) Branch current constraints [24]

$$I_l \leq I_{l,\max} \quad (5)$$

where I_l and $I_{l,\max}$ represent the maximum value of the current flowing through the l -th branch.

(4) Distributed power generation constraint [25]

$$\begin{cases} P_{DGi,\min} \leq P_{t,DGi} \leq P_{DGi,\max} \\ Q_{DGi,\min} \leq Q_{t,DGi} \leq Q_{DGi,\max} \end{cases} \quad (6)$$

where $P_{t,DGi}$ and $Q_{t,DGi}$ represent the active and reactive power injected by DG at the i -th node during the t -th period, respectively; $P_{DGi,\max}$ and $P_{DGi,\min}$ represent the upper and lower limits of the active power that the DG can supply to the i -th node, respectively; and $Q_{DGi,\max}$ and $Q_{DGi,\min}$ represent the upper and lower limits of the reactive power that the DG can supply to the i -th node, respectively.

2.3. Distributed Power Generation Model

(1) Wind Power Output

The wind power generation model is established according to [26], and the relationship between wind speed and output power at different times is shown in Equation (7).

$$P_w(v_t) = \begin{cases} 0 & (v_t < v_{ci}) \cup (v_t > v_{co}) \\ \frac{P_r}{v_r - v_{ci}}(v_t - v_{ci}) & (v_{ci} \leq v_t \leq v_r) \\ P_r & (v_r < v_t \leq v_{co}) \end{cases} \quad (7)$$

where P_r is the rated active power of the generator, v_t is the actual wind speed on site, v_{ci} is the minimum wind speed of the wind turbine, v_{co} is the maximum wind speed of the wind turbine, and v_r is the rated wind speed of the wind turbine.

(2) Photovoltaic Power Output

According to reference [27], the power output of photovoltaic cells is mainly related to the intensity of solar irradiance, the area of solar photovoltaic panels, and the photoelectric conversion efficiency. As the solar irradiance intensity follows a Beta distribution, its probability density function can be described as:

$$f(p_t) = \frac{\Gamma(\varepsilon + \beta)}{\Gamma(\varepsilon)\Gamma(\beta)} \left(\frac{p_t}{P_{\max}}\right)^{\varepsilon-1} \left(1 - \frac{p_t}{P_{\max}}\right)^{\beta-1} \quad (8)$$

where p_t represents the light intensity during period t , P_{\max} represents the upper limit of the power output capacity of the most comprehensive PV array in a given system, and ε and β represent parameters conforming to the Beta distribution.

The photovoltaic output power can be expressed as

$$P_{PV,t} = p_t \sum_{u=1}^U A_u \eta_u \quad (9)$$

where U is the total number of photovoltaic panels, A_u represents the u -th cell the area of the plate, and η_u represents the conversion efficiency of the battery plate.

3. Proposed Methodology

3.1. Time Division Method Based on the K-Means++ Clustering Algorithm

To address the issue of frequent reconfigurations in dynamic distribution networks, we employ the K-means++ [28,29] clustering algorithm to divide the daily load into periods, effectively reducing the active power loss and voltage offset and minimizing the number of reconfigurations.

Since the load status of each node in the distribution network changes dynamically with time, the load within 24 h is considered a dataset, with each dimension corresponding to the total number of nodes in the system. Using 1 h as a period, the node load of each period is treated as a sample set (O) for cluster analysis, $O = \{O_1, O_2, \dots, O_{24}\}$, $O_t = \{O_{t1}, O_{t2}, \dots, O_{tN}\}$, representing the apparent power of each node in the distribution network system within that period. During dynamic reconfiguration optimization, reconfiguration is carried out continuously, and interperiod reconfigurations must meet actual needs. Thus, distance segment constraints need to be added to cluster analysis, which is achieved as follows:

Step 1: Determine the collection dataset (O) using the elbow method to determine the optimal range of clustering, i.e., the K value.

Step 2: Randomly select a value from the sample dataset (O) as the initial value center and set the initial value of K to 1.

Step 3: Compute the Euclidean distance from each data object to the center of K . Using the roulette method, select the next cluster center.

Step 4: Repeat Step 3 until K initial value centers are generated.

Step 5: Divide the 24 moments in the sample dataset (O) into the nearest initial value center to form a cluster. Calculate the mean value of each dataset as the new initial value center.

Step 6: Repeat Step 5 until the sum of the squares of the distances from each data point to the corresponding cluster remains unchanged. Then, output the period in each group.

3.2. Dung Beetle Optimizer

The dung beetle optimizer takes inspiration from the biological behavior of dung beetles. The optimal solution is achieved by continuously updating the position updating formulas of four dung beetles, each with its position renewal formula, as follows:

The dung beetles that roll balls are updated and can be expressed as

$$x_i^{t+1} = x_i^t + \alpha \times k_1 \times x_i^{t-1} + k_2 \times \Delta x \quad (10)$$

Encountering obstacles, being unable to move forward, and repositioned dancing can be expressed as

$$x_i^{t+1} = x_i^t + \tan \theta |x_i^t - x_i^{t-1}| \quad (11)$$

The position-updating formulas for female dung beetles can be expressed as:

$$x_i^{t+1} = X^* + b_1 \times (x_i^t - Lb^*) + b_2 \times (x_i^t - Ub^*) \quad (12)$$

The position-updating formulas for small dung beetles can be expressed as:

$$x_i^{t+1} = x_i(t) + C_1 \times (x_i^t - Lb^b) + C_2 \times (x_i^t - Ub^b) \quad (13)$$

The position-updating formulas for thief dung beetles can be expressed as:

$$x_i^{t+1} = X^b + S \times g \times (|x_i^t - X^*| + |x_i^t - X^b|) \quad (14)$$

The values of k_1 and k_2 are fixed, with k_1 set to 0.1 and k_2 set to 0.3. The flexure angle ($\tan \theta$) belongs to the interval $[0, \pi]$ and is used in the position-updating formulas of the four dung beetles, where X^* and X^b represent the current best position and the global best position, respectively. The oviposition and reproduction areas have upper and lower limits represented by Ub^* , Lb^* , Ub^b , and Lb^b . The constants b_1 and b_2 represent independent random vectors of size $1 \times \text{dim}$. The variable C_1 is a random number drawn from a normal distribution, while C_2 is a random vector with values ranging from 0 to 1. Additionally, a random vector of size $1 \times \text{dim}$ that follows a normal distribution is represented by g , and S represents a constant value. The four dung beetle position-updating formulas are constantly updated until the optimal solution is found.

3.3. IMODBO Based on Mixed Strategy

After partitioning the data into time intervals, IMODBO is used to solve the distribution network reconstruction problem for each interval.

3.3.1. Population Initialization Based on a Tent Map

The standard dung beetle optimizer uses random initialization, which cannot guarantee the diversity of the population, affecting the quality of the global optimal solution. Using chaotic mapping to generate individuals randomly, the algorithm can effectively improve the speed and accuracy of the search for the optimal solution. As mentioned in [30], through many comparative experiments, chaotic tent mapping has better bias adaptation. The iteration equation of chaotic tent mapping is expressed as follows:

$$f(y_i) = \begin{cases} y_i/s & y_i \in (0, s) \\ (1 - y_i)/(1 - s) & y_i \in (s, 1) \end{cases} \quad 0 < s < 1 \quad (15)$$

Equation (15) shows that the chaotic tent mapping equation has fewer parameters, making the application convenient and straightforward. The population size is set to 500, the population dimension is to 2, and the parameter s is set to 0.5. The initial population distribution generated by chaotic tent mapping in the interval $[-100, 100]$ is shown in Figure 1. The initial population generated by chaotic tent mapping is distributed uniformly in space. Using these chaotic sequences, the initial population pop of the dung beetle algorithm can be obtained according to Equation (16).

$$pop = lb + (ub - lb) \times f(y_i) \quad (16)$$

In Equation (16), ub and lb are the upper and lower limits of the population.

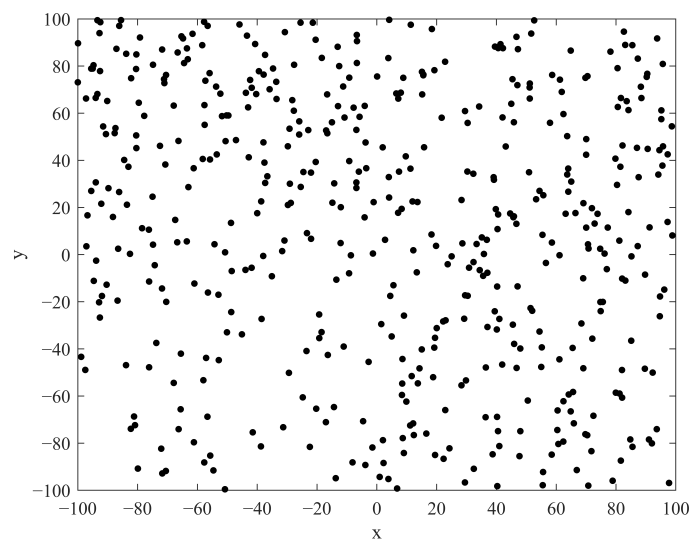


Figure 1. Initialization of the population using a chaos tent sequence.

3.3.2. Adaptive Weight Factor

According to the position-updating formula of the standard dung beetle optimizer, the four dung beetles strongly depend on the best position in the position-updating phase. Therefore, an adaptive weight factor is introduced in during the position updating, the formula of which is expressed as follows [31]:

$$W = W_{\max} - (W_{\max} - W_{\min}) \times (t^*/T_{\max}) \quad (17)$$

where W_{\max} is the maximum value of the adaptive weight, W_{\min} is the minimum value of the adaptive weight, T_{\max} represents the maximum number of iterations of the algorithm, and t^* indicates the current iteration number. After testing, the best algorithm performance is achieved when $W_{\max} = 0.9$ and $W_{\min} = 0.4$. As the number of iterations increases, the adaptive weight decreases from 0.9 to 0.4. At the beginning of the iteration, a more considerable adaptive weight improves the exploration ability of the algorithm. As the number of iterations increases, a smaller adaptive weight in the later stage improves the searchability of the algorithm. This prevents falling into a local optimum early, and the convergence in the last stage can gradually approach the optimal value. The position-updating equations are obtained by adding adaptive weighting factors into Equations (10)–(14), which can be expressed as follows:

The dung beetles that roll balls are updated and can be expressed as:

$$x_i^{t+1} = W \times x_i^t + \alpha \times k_1 \times x_i^{t-1} + k_2 \times \Delta x \quad (18)$$

$$x_i^{t+1} = W \times x_i^t + \tan \theta |x_i^t - x_i^{t-1}| \quad (19)$$

The position-updating formulas for female dung beetles can be expressed as:

$$x_i^{t+1} = W \times X^* + b_1 \times (x_i^t - Lb^*) + b_2 \times (x_i^t - Ub^*) \quad (20)$$

The position-updating formulas for small dung beetles are expressed as follows:

$$x_i^{t+1} = W \times x_i(t) + C_1 \times (x_i^t - Lb^b) + C_2 \times (x_i^t - Ub^b) \quad (21)$$

The position-updating formulas for thief dung beetles are expressed as follows:

$$x_i^{t+1} = W \times X^b + S \times g \times (|x_i^t - X^*| + |x_i^t - X^b|) \quad (22)$$

3.3.3. Levy Flight Disturbance Strategy and Variable Spiral Search Strategy

According to the characteristics of the ball-rolling dung beetle algorithm, the ball-rolling dung beetles can expand their search range by “dancing”. However, the search range of the three remaining dung beetles is relatively simple, so the Levy flight perturbation strategy and the variable spiral search strategy should be introduced to increase the global optimal search range. The Levy flight perturbation strategy is introduced, which enables the algorithm to search randomly at different distances, maximizes the diversification of the search domain, and enhances the optimal global searchability. Levy flight not only satisfies the small-scale refined search, ensuring that each target can be searched, but also satisfies the large-scale rough search, avoiding the limitations of local search. The distribution density function of the Levy flight step size change is expressed as [32]:

$$L(f) \sim |f|^{-1-\partial}, 0 < \partial \leq 2 \quad (23)$$

where f is the motion step of Levy flight, which can be expressed by Equation (24)

$$L_v = \frac{\mu}{|v|^{1/\partial}} \quad (24)$$

where μ and v are random numbers that conform to a normal distribution, and σ_μ and σ_v are obtained by Equation (25):

$$\begin{cases} \sigma_\mu = \left(\frac{\Gamma(1+\partial) \sin(\pi\partial/2)}{\Gamma[(1+\partial)/2]^2 \partial^{2(\partial-1)/2}} \right)^{1/\partial} \\ \sigma_v = 1 \end{cases} \quad (25)$$

where the value range of parameter ∂ is $0 < \partial < 2$, and generally, $\partial = 1.5$.

The variable helical search strategy allows for the development of various position-updating search paths, balancing the global and local searches of the algorithm. In the position-updating process, the parameter z is designed as an adaptive variable to solve the monotony of the spiral parameter in the search method in case of falling into a locally optimal solution. It is used to dynamically adjust the spiral shape of the three dung beetle searches, thereby broadening the ability of three dung beetles to explore unknown areas and improving the algorithm's search efficiency and global search performance. The formula for the variable helical search strategy is as follows [33]:

$$Q = e^{zh} \times \cos(2\pi h) \quad (26)$$

where Q is the spiral factor, and h is the random number of $(-1, 1)$, where $z = e^{k \cdot \cos((t^*/T_{max}) \cdot \pi)}$, and $k = 5$.

In summary, the position updates of the four improved dung beetles are expressed as follows:

The position-updating formulas for the dung beetles that roll balls are updated and can be expressed as:

$$x_i^{t+1} = W \times x_i^t + \alpha \times k_1 \times x_i^{t-1} + k_2 \times \Delta x \quad (27)$$

$$x_i^{t+1} = W \times x_i^t + \tan \theta |x_i^t - x_i^{t-1}| \quad (28)$$

The position-updating formulas for female dung beetles can be expressed as:

$$x_i^{t+1} = W \times X^* + Q \times [b_1 \times (x_i^t - Lb^*) + b_2 \times (x_i^t - Ub^*)] \quad (29)$$

The position-updating formulas for small dung beetles are expressed as follows:

$$x_i^{t+1} = W \times x_i(t) + Q \times [C_1 \times (x_i^t - Lb^b) + C_2 \times (x_i^t - Ub^b)] \quad (30)$$

The position-updating formulas for thief dung beetles are expressed as follows:

$$x_i^{t+1} = L_v \times W \times X^b + S \times g \times (|x_i^t - X^*| + |x_i^t - X^b|) \quad (31)$$

3.4. Pareto Dominance Theory

The traditional dung beetle optimizer selection strategy is suitable for single-objective optimization problems but not for multi-objective distribution network optimization and reconstruction problems. Therefore, in this paper, we use the Pareto dominance theory to evaluate the solutions generated by the distribution network optimization and reconstruction problem. Individuals with high degrees of optimization and extensive coverage ranges are selected to form the population for the next iteration. According to the Pareto theory, the objective function of this iteration is ranked by non-dominant levels. Every time a fitness calculation is performed, it is compared with the solution set. The solution with the highest non-dominant level is stored in the external archive as the current optimal solution, and solutions with lower non-dominant levels are removed. This process is repeated until the fitness calculation is completed.

Step 1 involves reading the distribution network data and determining the loop and the branch switches of each loop participating in the coding.

Step 2 sets the initial parameters, including the number of populations, the maximum number of iterations (T), the population dimension (dim), and the upper and lower limits of each dimension component of IMODBO based on the number of branch switches of each loop participating in the encoding.

Step 3 generates the population using the chaotic tent map according to Equation (16).

Step 4 calculates the fitness of each individual in the population, performs Pareto screening, selects the solution with the highest non-domination level, and stores it in an external file.

Step 5 divides the population into four types of dung beetles and updates the positions of the four dung beetles according to Equations (27)–(31).

Step 6 recalculates the fitness of the updated positions, compares them with the external file using greedy selection, and updates the external file.

Step 7 checks whether the current iteration number of the algorithm reaches T. If not, the algorithm proceeds to Step 8; otherwise, it returns to Step 4.

Step 8 outputs the optimal solution from the external file.

In summary, the steps of the improved multi-objective dung beetle algorithm for solving distribution network optimization and reconstruction problems are shown in the Figure 2.

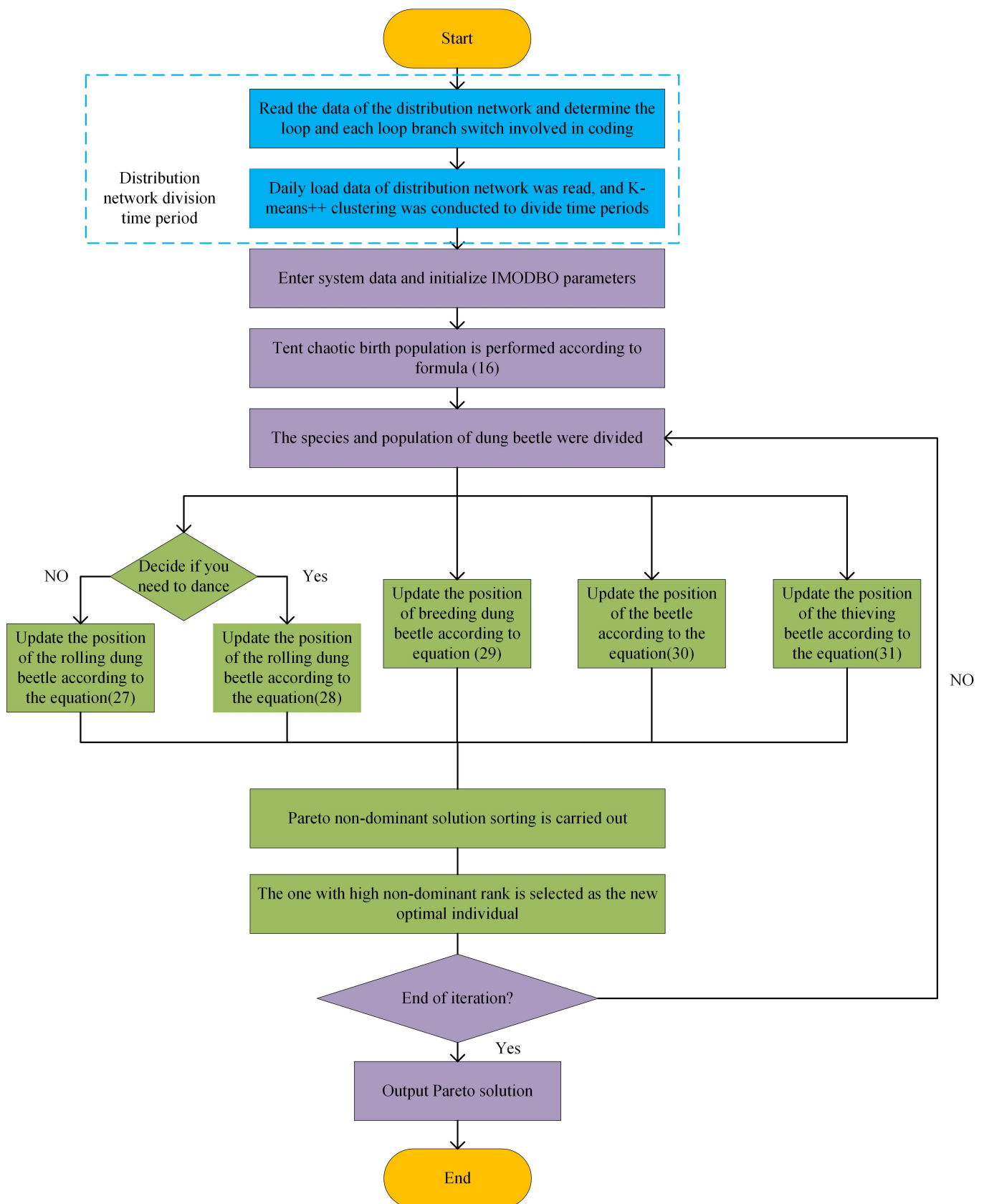


Figure 2. Flow chart of the process for solving the dynamic reconfiguration of the distribution network with distributed generation based on IMODBO.

4. Result and Discussion

In this study, we conducted performance testing on the algorithm using both single-objective and multi-objective test functions. A comparison was made between IMODBO and existing algorithms. Furthermore, a comparative analysis was performed on two distribution network systems through multiple experimental comparisons.

4.1. IMODBO Performance Testing

To verify the effectiveness of the IMODBO algorithm, a simulation comparison experiment was carried out on the algorithm, and the algorithm's performance was tested using test functions. The population size of each test function was set to 300, and the maximum number of iterations was set to 50. Function expressions are shown in Table 1. The following algorithm was used for comparative experiments. Whale optimization algorithm (WOA) [34], gray wolf optimizer (GWO) [35], northern goshawk optimization (NGO) [36], and improved salp swarm algorithm (ISSA) [37], as well as multi-objective algorithms non-dominated sorting genetic algorithm II (NSGA-II) [38], multi-objective ant lion optimizer (MOALO) [39], multi-objective dragonfly algorithm (MODA) [40], multi-objective slime mold algorithm (MOSMA) [41], multi-objective particle swarm optimization (MOPSO) [42,43], and the multi-objective whale optimization algorithm (MOWOA) [44].

Table 1. Classic test function.

Name	Function	Interval
$f_1(x)$	$\sum_{i=1}^n x_i^2$	$[-100, 100]$
$f_2(x)$	$\sum_{i=1}^n x_i + \prod_{i=1}^n x_i $	$[-10, 10]$
$f_3(x)$	$\frac{1}{4000} \sum_{i=1}^n x_i^2 - \prod_{i=1}^n \cos(\frac{x_i}{\sqrt{i}})$	$[-600, 600]$
$f_4(x)$	$\max_i \{ x_i , 1 \leq i \leq n\}$	$[-100, 100]$
ZTD1	$\begin{cases} f_1 = x_1, f_2 = g \left(1 - \sqrt{\frac{x_1}{g}}\right) \\ g = 1 + 9 \sum_{i=2}^n x_i/n - 1 \end{cases}$	$[0, 1]$
ZTD2	$\begin{cases} f_1 = x_1, f_2 = g \left(1 - \left(\frac{x_1}{g}\right)^2\right) \\ g = 1 + 9 \sum_{i=2}^n x_i/n - 1 \end{cases}$	$[0, 1]$
ZTD3	$\begin{cases} f_1 = x_1, g = 1 + 9 \sum_{i=2}^n x_i/n - 1 \\ f_2 = g \left(1 - \sqrt{\frac{x_1}{g}} - \frac{x_1}{g} \sin(10\pi x_1)\right) \end{cases}$	$[0, 1]$
ZTD4	$\begin{cases} f_1 = x_1, f_2 = g \left(1 - \sqrt{\frac{f_1}{g}}\right) \\ g = 1 + 10(m-1) + \sum_{i=2}^m (x_i^2 - 10 \cos(4\pi x_i)) \end{cases}$	$[0, 1]$

4.1.1. Test Functions and Performance Evaluation

The multi-objective intelligent algorithm was evaluated with three evaluation indices. The specific calculation methods for each index are as follows:

(1) Inverted Generational Distance Indicator

The inverted generational distance (IGD) indicator is commonly used to evaluate the convergence and diversity of the non-dominated solutions obtained by the algorithm. It measures the average Euclidean distance between all solutions in the Pareto front and the non-dominated solutions. A low IGD value indicates the better convergence and diversity of the algorithm. The calculation formula of IGD is as follows [45]:

$$IGD(P, P^*) = \frac{\sum_{h \in P} d(h, P^*)}{|pop|} \quad (32)$$

where P is the distribution of a real set of points on the Pareto frontier, $|pop|$ represents the number of set points pop , P^* for the algorithm to obtain the Pareto optimal solution set, and $d(h, P^*)$ represents the minimum Euclidean distance from a point in the set.

(2) Hypervolume Indicator

The hypervolume (HV) metric is used to evaluate the quality of the non-dominated solution set generated by the algorithm concerning a reference point. A high HV value indicates better comprehensive algorithm performance in developing well-distributed and diverse non-dominated solutions. The calculation formula of HV is as follows [46]:

$$HV = \lambda(U_{i=1}^{|P^*|} v_i) \quad (33)$$

where λ represents the Lebesgue measure, and v_i represents the super volume formed by the reference point.

(3) Spacing

To evaluate the diversity of the solution set, the standard deviation of the minimum distance from each solution to the other solutions is calculated, which is commonly referred to as the spacing metric. A low spacing value indicates a more uniform distribution of solutions in the objective space. The calculation formula of spacing is as follows [47]:

$$SP = \sqrt{\frac{1}{|pop| - 1} \sum_{i=1}^{|pop|} (\bar{d} - d_i)^2} \quad (34)$$

where d_i and \bar{d} represent the minimum distance from the i -th solution to other solutions and the average value of d_i , respectively.

The single-objective test function was calculated, and the results of the experiment are presented in Table 2. Additionally, the iteration curve is depicted in Figure 3.

Table 2. Test results of six optimization algorithms.

F	Index	IMODBO	DBO	ISSA	NGO	WOA	GWO
$f_1(x)$	Worst	0	2.25×10^{-71}	7.59×10^{-23}	1.11×10^{-50}	2.636×10^{-49}	1.227×10^{-17}
	Best	0	4.60×10^{-99}	2.61×10^{-23}	2.24×10^{-53}	3.56×10^{-58}	1.10×10^{-19}
	Ave	0	7.21×10^{-73}	4.92×10^{-23}	1.69×10^{-51}	1.81×10^{-50}	1.95×10^{-18}
	Std	0	3.31×10^{-72}	1.28×10^{-23}	2.2×10^{-51}	4.81×10^{-50}	2.33×10^{-18}
$f_2(x)$	Worst	2.70×10^{-204}	4.49×10^{-29}	3.44×10^{-12}	1.26×10^{-26}	2.24×10^{-31}	4.85×10^{-11}
	Best	4.02×10^{-268}	7.76×10^{-56}	1.81×10^{-512}	1.60×10^{-27}	2.39×10^{-40}	6.25×10^{-12}
	Ave	5.40×10^{-206}	1.15×10^{-30}	2.83×10^{-12}	5.04×10^{-27}	1.79×10^{-32}	2.07×10^{-11}
	Std	0	6.55×10^{-30}	3.98×10^{-13}	2.50×10^{-27}	4.90×10^{-32}	1.09×10^{-11}
$f_3(x)$	Worst	0	3.45×10^{-2}	6.64×10^{-1}	0	2.53×10^{-1}	2.73×10^{-2}
	Best	0	0	0	0	0	0
	Ave	0	1.04×10^{-3}	4.62×10^{-2}	0	1.94×10^{-2}	4.82×10^{-3}
	Std	0	5.41×10^{-3}	1.41×10^{-1}	0	5.99×10^{-2}	8.65×10^{-3}
$f_4(x)$	Worst	1.42×10^{-54}	1.66×10^{-22}	5.03×10^{-12}	1.50×10^{-21}	87.3612	7.16×10^{-4}
	Best	1.05×10^{-257}	3.84×10^{-49}	2.03×10^{-12}	1.10×10^{-22}	1.09×10^{-2}	2.28×10^{-2}
	Ave	4.11×10^{-56}	3.32×10^{-24}	3.32×10^{-12}	4.59×10^{-22}	47.8064	1.28×10^{-4}
	Std	2.10×10^{-55}	2.35×10^{-23}	6.32×10^{-13}	2.87×10^{-22}	28.4172	1.17×10^{-4}

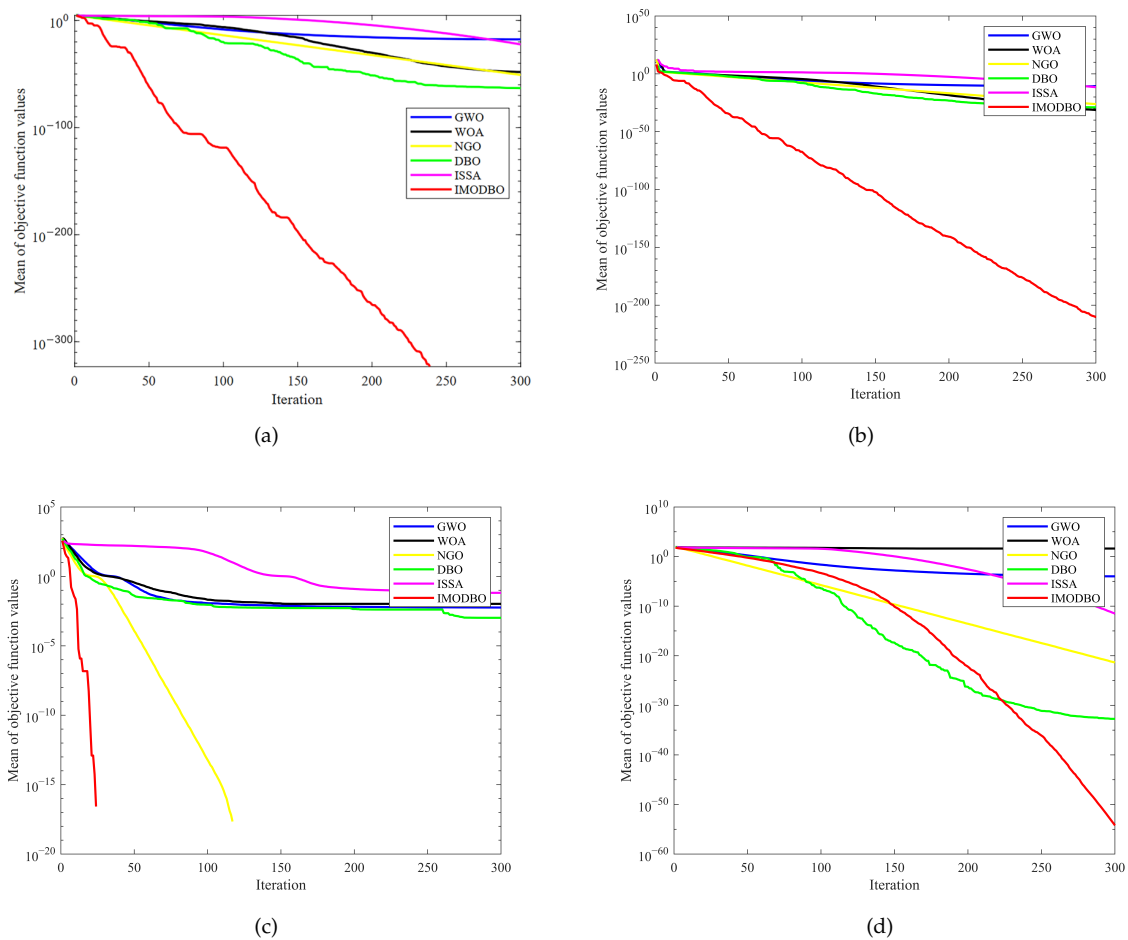


Figure 3. (a) $f_1(x)$; (b) $f_2(x)$; (c) $f_3(x)$; (d) $f_4(x)$.

4.1.2. Analysis of Test Results

According to the data in Table 2, the performance of IMODBO on different test functions far exceeds those of other algorithms, and according to Figure 3, IMODBO only required a small number of iterations to find the optimal solution. The results show that the introduction of different strategies can greatly improve the optimization accuracy of the algorithm and improve the performance of the algorithm.

The calculation results of the three indices are shown in Tables 3–5. The Pareto front solutions of seven different multi-objective algorithms on each test function and the accurate Pareto front distribution of the test function are shown in Figure 4.

Tables 3–5 show three comprehensive indices of each algorithm under different test functions. According to the IGD index, IMODBO performs well on all four test functions, with only slightly inferior performance to that of MOWOA on the ZDT4 function, indicating that IMODBO has a strong searching ability. According to the HV index, the results obtained by IMODBO are similar to those obtained by MOWOA and MOSMA but better than the results obtained by the other algorithms, indicating that IMODBO has a rich solution diversity and the best all-around performance. From the perspective of the SP index, IMODBO has the best solution distribution space, widest solution set distribution, and best distribution performance. Based on the performance indices obtained from the test function, the IMODBO algorithm has apparent advantages in terms of distribution and convergence.

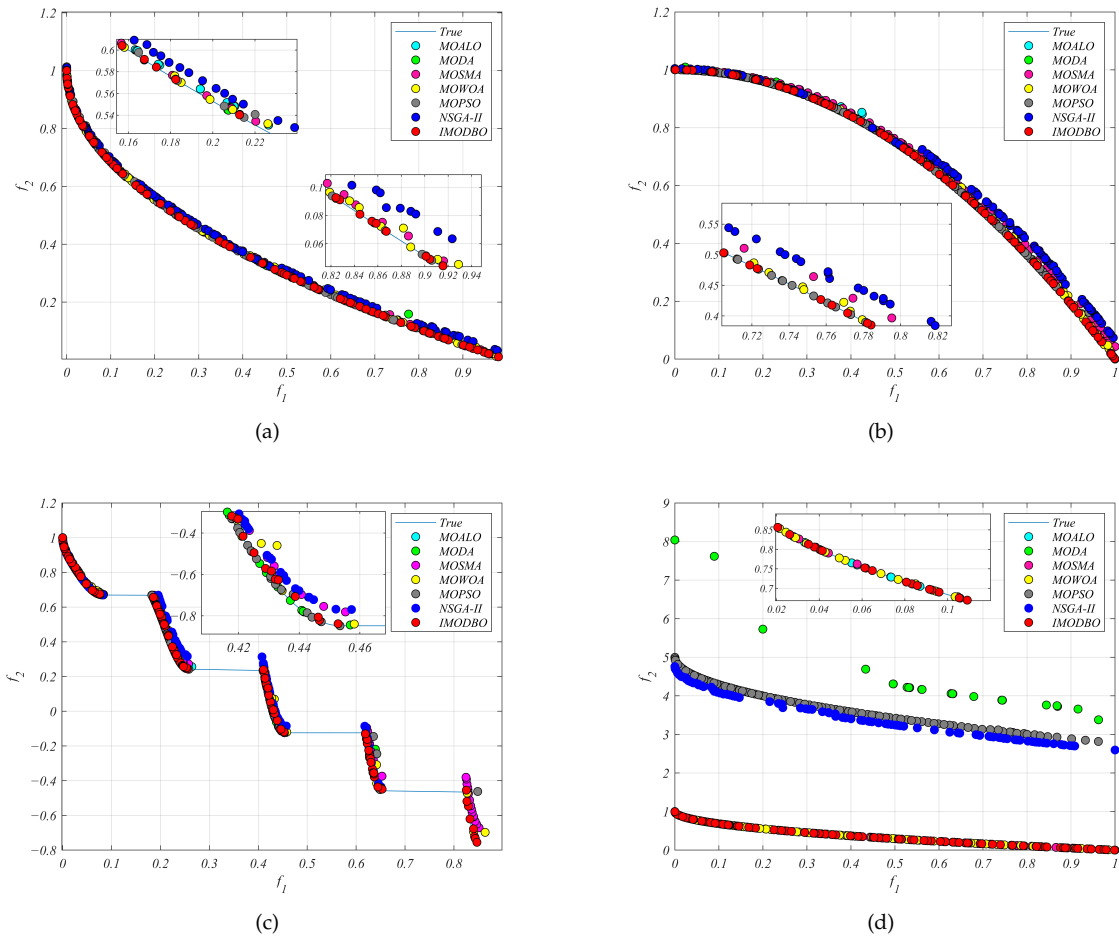


Figure 4. (a) ZDT1 Pareto solutions; (b) ZDT2 Pareto solutions; (c) ZDT3 Pareto solutions; and (d) ZDT4 Pareto solutions.

Table 3. IGD calculation result.

Algorithm	ZDT1	ZDT2	ZDT3	ZDT4
IMODBO	7.01×10^{-3}	1.76×10^{-1}	8.32×10^{-3}	6.31×10^{-3}
NSGA-II	1.57×10^{-2}	2.96×10^{-1}	1.35×10^{-1}	2.34
MOALO	3.28×10^{-2}	2.90×10^{-1}	2.67×10^{-2}	4.02×10^{-2}
MODA	5.23×10^{-2}	2.86×10^{-1}	2.57×10^{-2}	2.84
MOSMA	7.12×10^{-3}	2.90×10^{-1}	2.54×10^{-2}	8.68×10^{-3}
MOWOA	7.21×10^{-3}	2.85×10^{-1}	2.46×10^{-2}	6.10×10^{-3}
MOPSO	2.71×10^{-2}	1.89×10^{-1}	2.46×10^{-2}	2.55

Table 4. HD calculation result.

Algorithm	ZDT1	ZDT2	ZDT3	ZDT4
IMODBO	7.16×10^{-1}	4.41×10^{-1}	3.93×10^{-1}	3.98×10^{-1}
NSGA-II	4.02×10^{-1}	2.14×10^{-1}	2.97×10^{-1}	0
MOALO	3.99×10^{-1}	1.06×10^{-1}	4.39×10^{-1}	3.72×10^{-1}
MODA	3.75×10^{-1}	9.97×10^{-2}	3.83×10^{-1}	0
MOSMA	3.98×10^{-1}	1.08×10^{-1}	2.98×10^{-1}	3.98×10^{-1}
MOWOA	4.08×10^{-1}	1.12×10^{-1}	2.99×10^{-1}	4.05×10^{-1}
MOPSO	7.15×10^{-1}	2.85×10^{-1}	6.83×10^{-1}	0

Table 5. SP calculation result.

Algorithm	ZDT1	ZDT2	ZDT3	ZDT4
IMODBO	4.73×10^{-3}	5.43×10^{-3}	1.01×10^{-2}	9.64×10^{-3}
NSGA-II	9.24×10^{-3}	1.14×10^{-2}	1.56×10^{-2}	2.25×10^{-2}
MOALO	5.10×10^{-3}	6.50×10^{-3}	1.28×10^{-2}	1.30×10^{-2}
MODA	2.89×10^{-2}	1.00×10^{-2}	3.11×10^{-2}	3.12×10^{-2}
MOSMA	1.21×10^{-2}	9.45×10^{-3}	1.24×10^{-2}	8.77×10^{-3}
MOWOA	1.19×10^{-2}	6.42×10^{-3}	2.99×10^{-2}	6.73×10^{-3}
MOPSO	1.33×10^{-2}	2.85×10^{-1}	2.42×10^{-2}	1.08×10^{-2}

4.2. Reconstruction of the IEEE 33 and PG&E 69 Power Distribution Systems

We conducted simulation verification tests using MATLAB R2022a on the IEEE 33 [48] and PG&E 69 [49] power distribution systems. The proposed method was validated on the IEEE 33-node power distribution system to demonstrate its effectiveness and was further applied to the PG&E 69 distribution system to showcase its universality. Two sets of comparative experiments were conducted on each distribution network system as follows:

- The K-means++ clustering algorithm was employed to divide the distribution network load dataset into different time periods, facilitating comparative analyses under various scenarios.
- A comprehensive test was conducted during a single time period to compare the performance of IMODBO with various other algorithms.

4.2.1. IEEE 33-Node System Reconstruction

As shown in Figure 5, the IEEE 33-node system contains five contact switches, 37 branches, and 33 nodes. Wind power generation was connected to nodes 8 and 18, and photovoltaic cells were connected to node 32. The load added to DG was calculated according to Tables 6 and 7.

Table 6. Photovoltaic cell parameters.

Solar Cell	A/m^2	η	$p_{\max}/(W/m^2)$
PV	4500	15	20

Table 7. Wind turbine parameters.

Wind Turbine Set	P_r/kW	$v_{ci}/(m/s)$	$v_r/(m/s)$	$v_{co}/(m/s)$
W_1	500	3.5	14.5	20
W_2	600	3.0	13.0	19

The dynamic reconfiguration analysis of the distribution network was carried out, and the load distribution of the distributed power supply was added, as shown in Figure 6. The load is different at each moment and each node, which includes commercial, residential, and industrial loads. A load of each period was calculated according to Equation (35) to simulate the dynamic operation of the distribution network. The daily load variation curve of the IEEE 33-node distribution network system is shown in Figure 7.

$$L_{i,t} = \sum_{h=1}^3 L_{i,\max} H_{i,h} C_{h,t} \quad (35)$$

where i is the node number, t is the time point, h is the load type, $L_{i,\max}$ is the peak load of the i -th node, $H_{i,h}$ is the proportion of the class h load in the i -th node, and $C_{h,t}$ is the proportion of the class h load during the t -th period. We take 110% of the standard load peak value of IEEE 33-nodes. The period was divided using the elbow method and the

K-means++ clustering algorithm. The inflection point was determined to be 4, and the time period was divided into four class clusters, as shown in Figure 8.

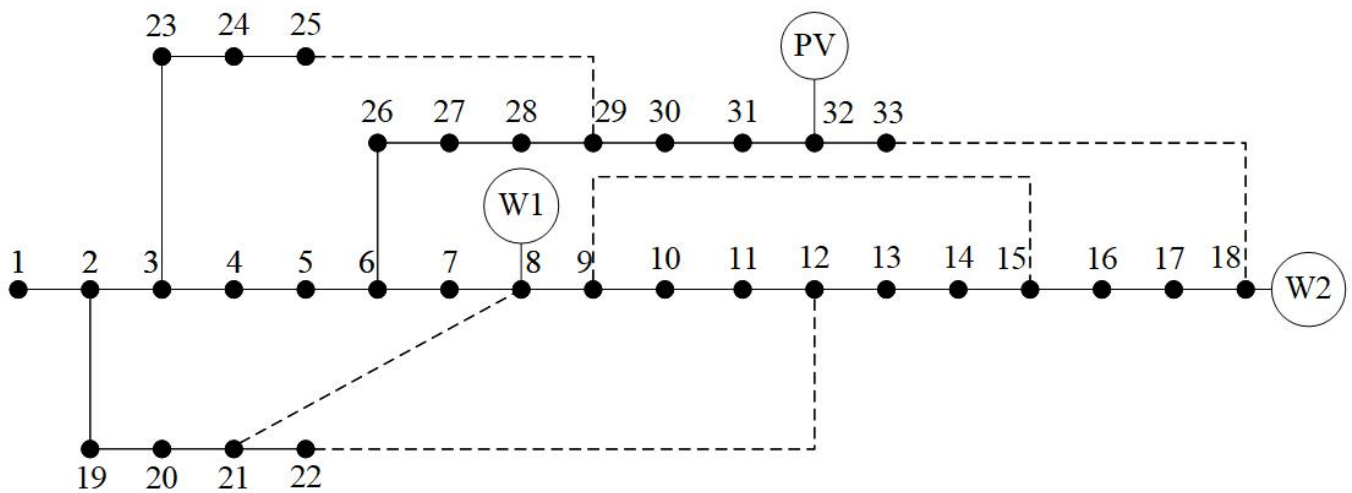


Figure 5. IEEE 33-node diagram.

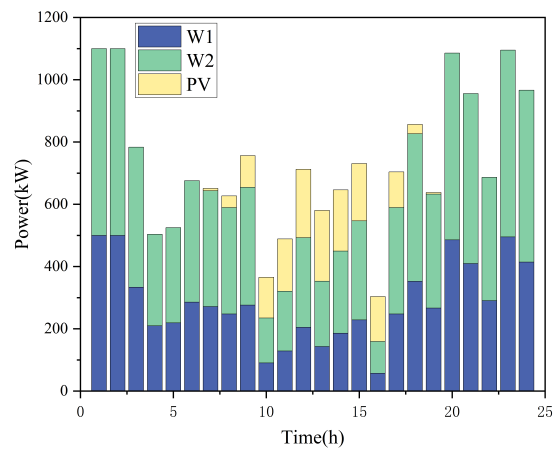


Figure 6. Different distributed power supply loads.

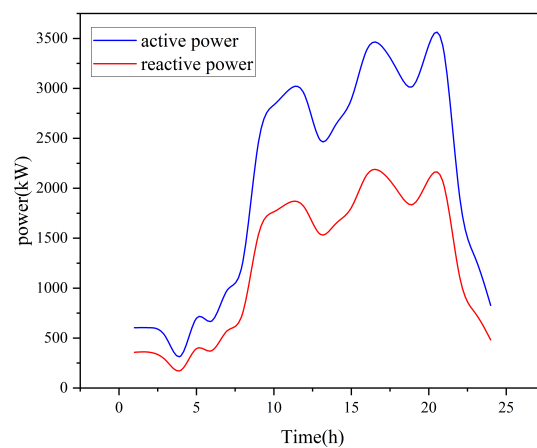


Figure 7. Daily load variation.

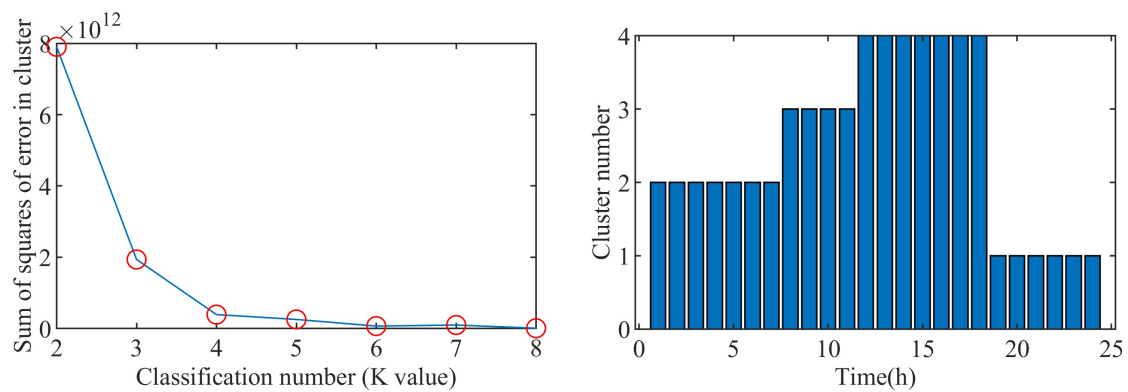


Figure 8. Period division.

Three scenarios were set up for comparative analysis:

Scenario 1: Maintain the original system structure without reconfiguration;

Scenario 2: Use IMODBO to reconfigure once every period;

Scenario 3: Dynamic reconfiguration via IMODBO.

The final operation effect is shown in Table 8.

Table 8. Result comparison after reconfiguration.

Scenario	Time Period	Disconnect Branch	Active Network Loss /kW	Voltage Offset /p.u
Scenario 1	24 h	8-4-2-4-4	1492.14	17.3396
	0.00–1.00	5-7-21-12-15		
	1.00–2.00	33-7-35-12-37		
	2.00–3.00	28-20-35-12-30		
	3.00–4.00	28-6-11-12-30		
	4.00–5.00	27-7-10-13-30		
	5.00–6.00	28-7-9-12-15		
	6.00–7.00	28-7-11-14-16		
	7.00–8.00	26-7-21-12-17		
	8.00–9.00	28-7-9-12-16		
	9.00–10.00	28-7-9-14-17		
	10.00–11.00	28-7-9-12-17		
	11.00–12.00	28-7-9-13-17		
Scenario 2	12.00–13.00	28-7-21-13-15	1105.74	12.3715
	13.00–14.00	28-7-9-14-17		
	14.00–15.00	28-7-11-14-17		
	15.00–16.00	28-7-9-14-17		
	16.00–17.00	27-7-35-14-32		
	17.00–18.00	28-7-9-12-32		
	18.00–19.00	28-7-9-14-17		
	19.00–20.00	28-7-9-13-16		
	20.00–21.00	28-7-10-14-16		
	21.00–22.00	28-7-11-14-31		
	22.00–23.00	28-6-11-13-31		
	23.00–24.00	27-7-11-14-15		
Scenario 3	0.00–7.00	3-7-9-12-15	1090.4	12.1026
	8.00–11.00	28-7-11-14-15		
	12.00–18.00	28-7-9-14-17		
	19.00–24.00	28-7-9-13-31		

By comparing the data in Scenario 1 and Scenario 2 in Table 8, we can see that, if the distribution network system is not reconfigured and optimized, the overall network loss and

voltage offset are relatively high. Dynamic reconfiguration using the IMODBO proposed in this paper can effectively reduce the functional network loss and voltage offset. Before reconfiguration, the active network loss is 1492.14 kW; after reconfiguration, the active network loss is 1105.74 kW. The voltage offset before reconfiguration is 17.3396 $p.u.$, and after reconfiguration, the voltage offset is 12.3715 $p.u.$, which is 30.2% lower than without reconfiguration. The effect is remarkable. A comparison of Scenario 2 with Scenario 3 shows that the daily load in Scenario 2 is divided into 24 periods and reconstructed once each period, leading to a slower reconfiguration speed and more switching actions. In Scenario 3, the active power network loss is 15.34 kW lower than that in Scenario 2. The voltage offset decreases by 0.22 $p.u.$ from 12.3715 $p.u.$ to 12.1026 $p.u.$

The above results show that the method proposed in this paper reduces the number of switching actions and ensures calculation accuracy. Figure 9 shows that Scenario 3 can effectively minimize the work packet loss in most periods. Figures 10–12 show that the node voltage distribution in Scenario 3 is more uniform.

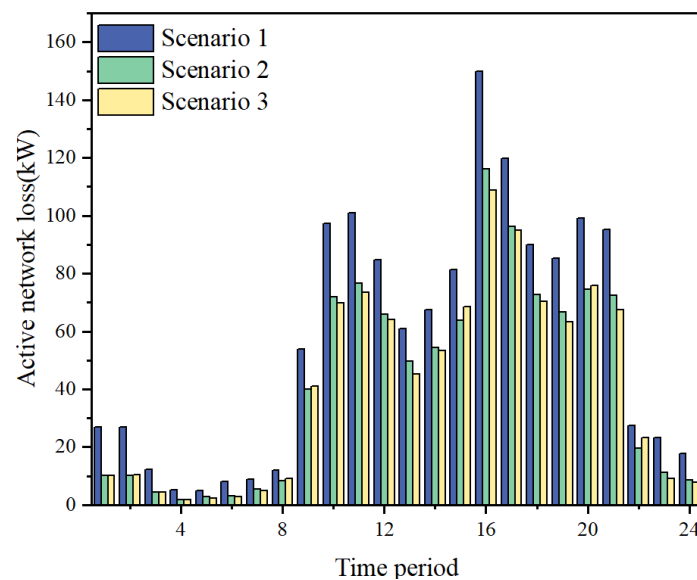


Figure 9. Active network loss corresponding to each scenario.

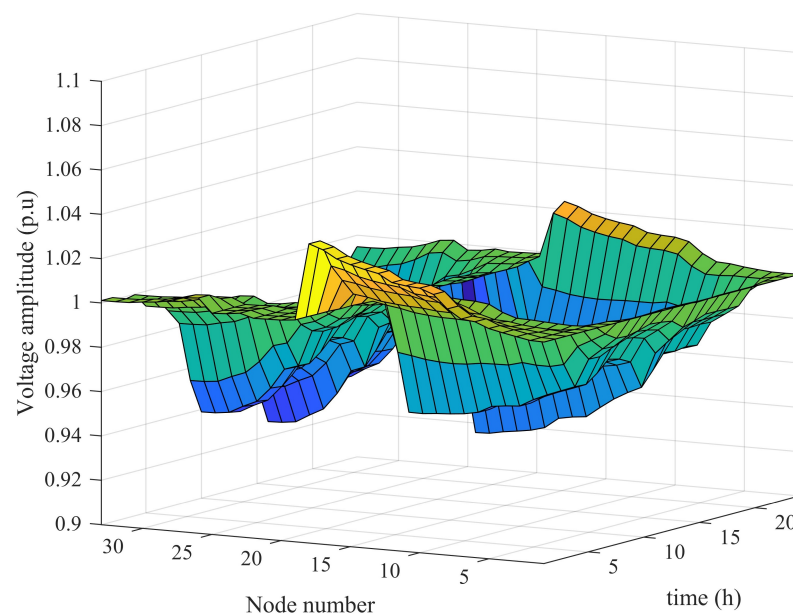


Figure 10. Scenario 1 —node voltage distribution.

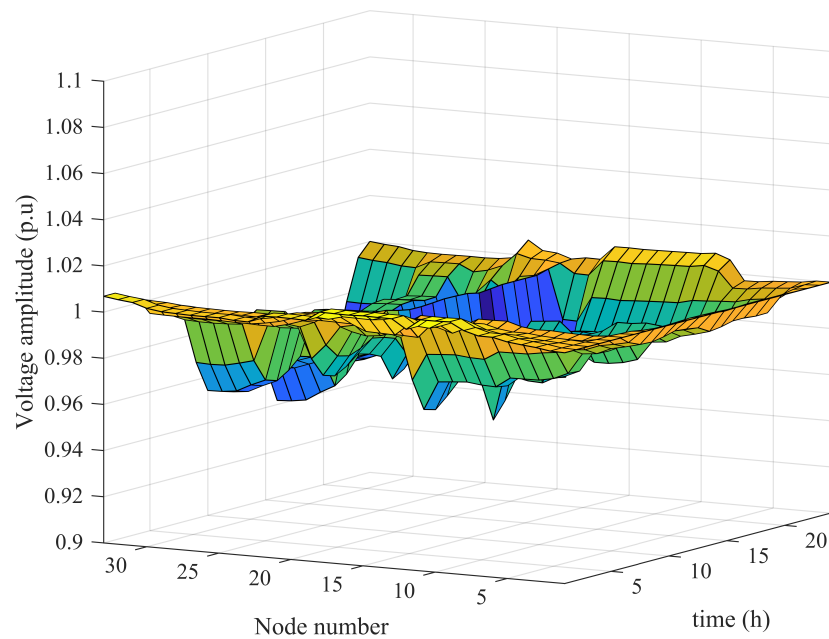


Figure 11. Scenario 2—node voltage distribution.

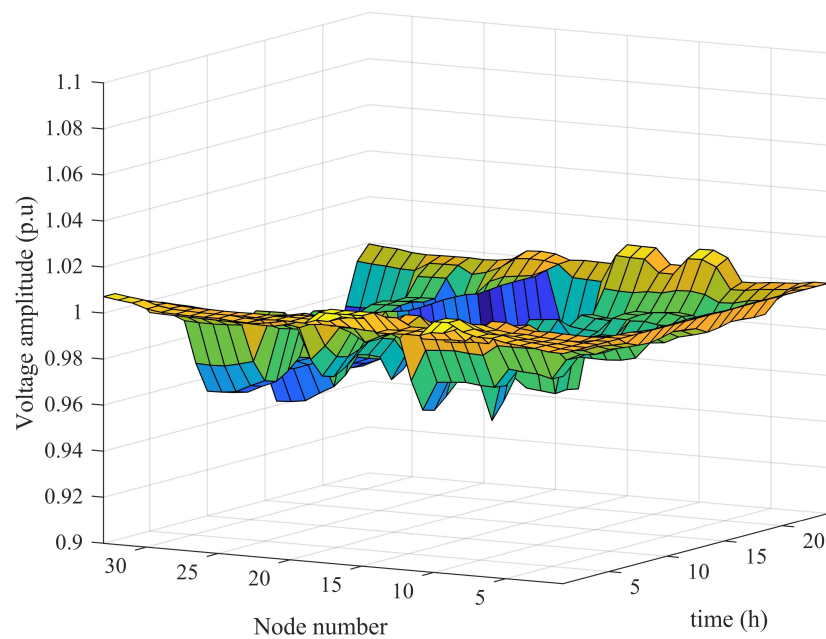


Figure 12. Scenario 3—node voltage distribution.

4.2.2. PG&E 69-Node System Reconstruction

The PG&E 69-node distribution system is shown in Figure 13. Wind power generation is connected to nodes 33 and 64, and photovoltaic cells are connected to node 14. The load of the connected distributed power supply is the same as previously described. The daily load curve of the PG&E 69-node distribution system is shown in Figure 14.

The time period is divided according to the algorithm described in Section 2, setting the same scene as the IEEE 33-nodes. Table 9 shows the final running effect.

Table 9. Result comparison after reconfiguration.

Scenario	Time Period	Disconnect Branch	Active Network Loss /kW	Voltage Offset /p.u	
Scenario 1	24 h	7–8–24–32–17	2315.17	24.7262	
	1.00–2.00	7–19–13–50–47			
	2.00–3.00	10–19–14–50–47			
	3.00–4.00	10–19–14–50–47			
	4.00–5.00	8–19–14–50–47			
	5.00–6.00	10–19–14–52–47			
	6.00–7.00	63–18–14–53–47			
	7.00–8.00	10–19–14–52–47			
	8.00–9.00	8–19–14–51–47			
	9.00–10.00	69–70–13–53–47			
	10.00–11.00	10–19–14–52–47			
	Scenario 2	11.00–12.00	69–19–14–51–47	1134.09	12.6591
		12.00–13.00	10–19–14–50–47		
		13.00–14.00	10–19–14–53–47		
		14.00–15.00	10–19–14–53–47		
		15.00–16.00	10–19–14–51–47		
		16.00–17.00	10–19–14–53–47		
		17.00–18.00	10–19–14–53–47		
		18.00–19.00	9–19–14–50–47		
		19.00–20.00	10–19–14–51–47		
		20.00–21.00	63–19–14–50–47		
		21.00–22.00	10–19–14–50–47		
		22.00–23.00	10–70–13–50–44		
		23.00–24.00	10–19–14–52–47		
Scenario 3		0.00–7.00	7–19–14–50–7		
	8.00–11.00	10–19–14–52–47	1120.81	11.3161	
	12.00–18.00	63–19–14–50–47			
	19.00–24.00	10–19–14–53–47			

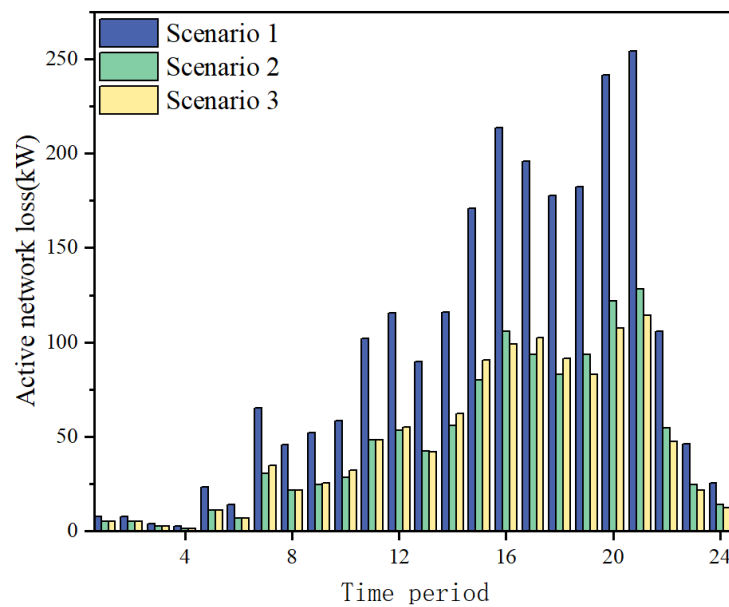


Figure 15. Active network loss corresponding to each scenario.

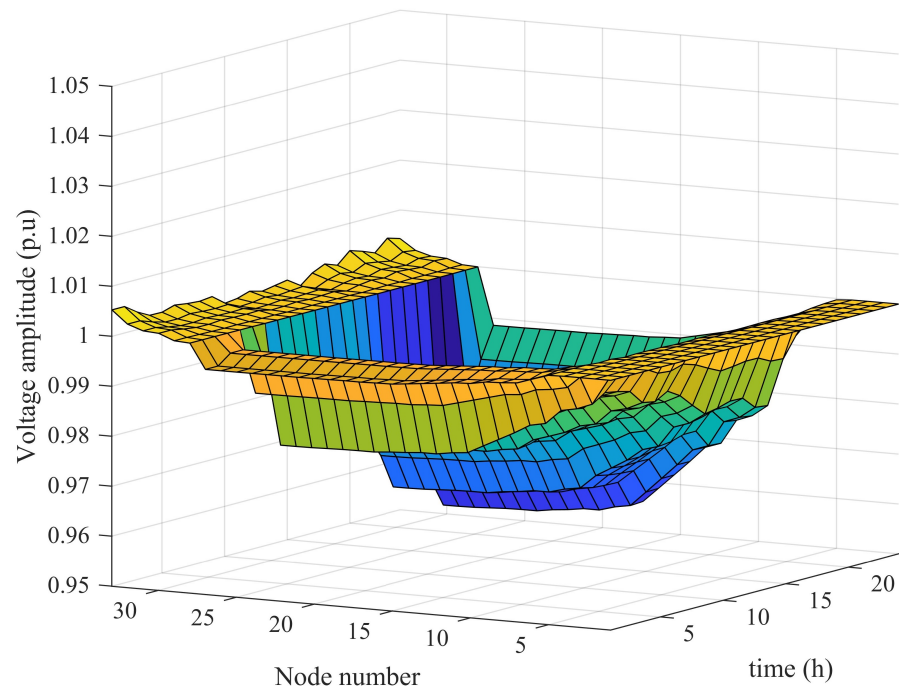


Figure 16. Scenario 1—node voltage distribution.

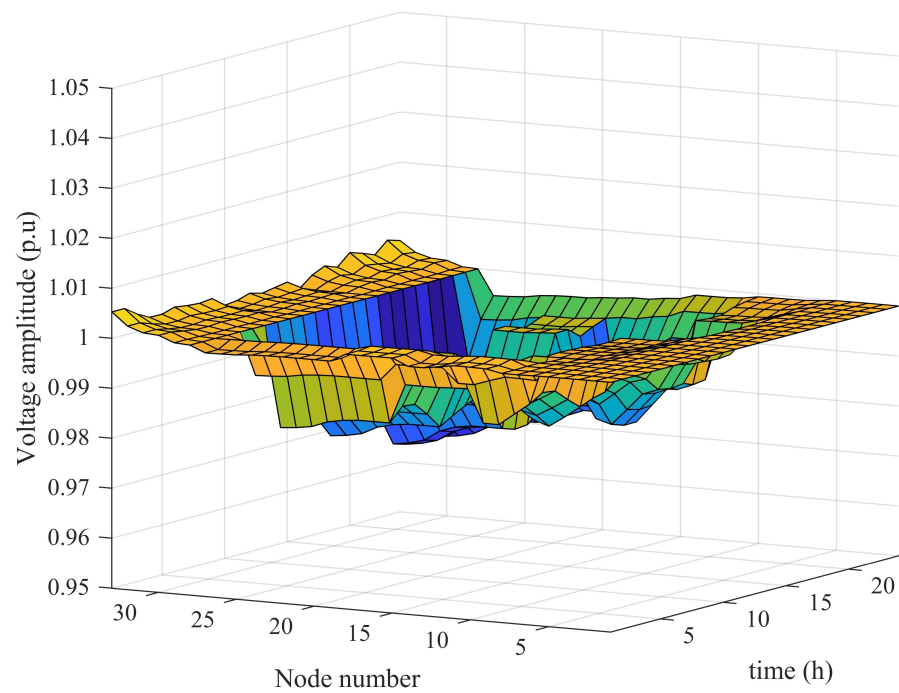


Figure 17. Scenario 2—node voltage distribution.

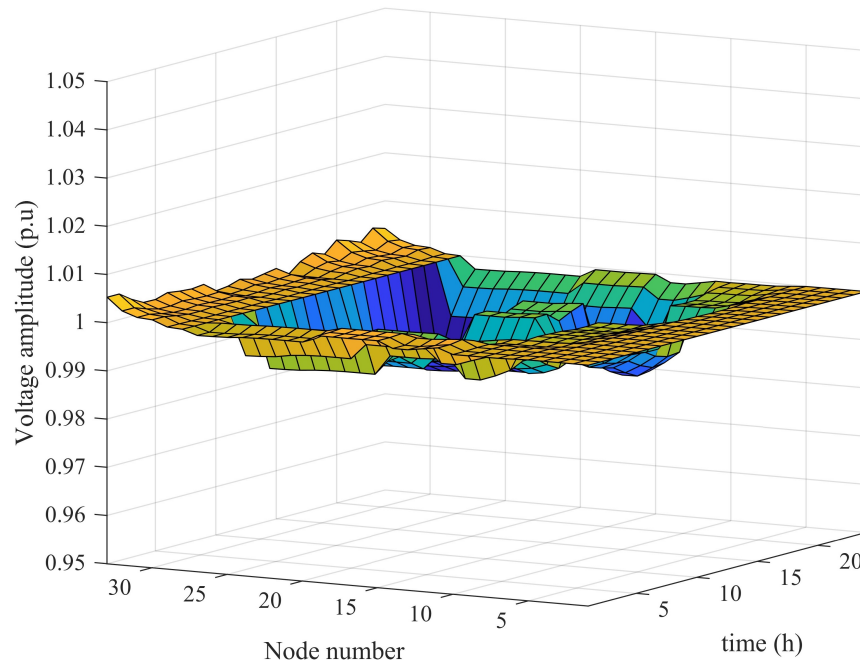


Figure 18. Scenario 3—node voltage distribution.

4.2.3. Comparison Test of Different Algorithms

To verify the effectiveness of the IMODBO in the dynamic reconfiguration of a distributed power distribution network, the NSGA-II, MOALO, MOPSO algorithms were used in this study to compare the solution results of the IEEE 33-node and PG69-node system models and distributed power supply.

Because the real Pareto solution set in the system cannot be known, the four algorithms were run independently ten times, and their Pareto solution sets were taken for non-dominated sorting to simulate the natural Pareto frontier of the IEEE 33-node distribution network. Taking the distribution network load in the eighth hour as an example, the Pareto solution set obtained after the four-stage algorithm was run, as shown in Figure 19. To further demonstrate the effectiveness of the approach, the Pareto solution set for the PG&E 69-node distribution network during the fourteenth hour is also presented. Moreover, two multi-objective performance indicators are calculated, as shown in Table 10, through which the performances of different algorithms can be judged.

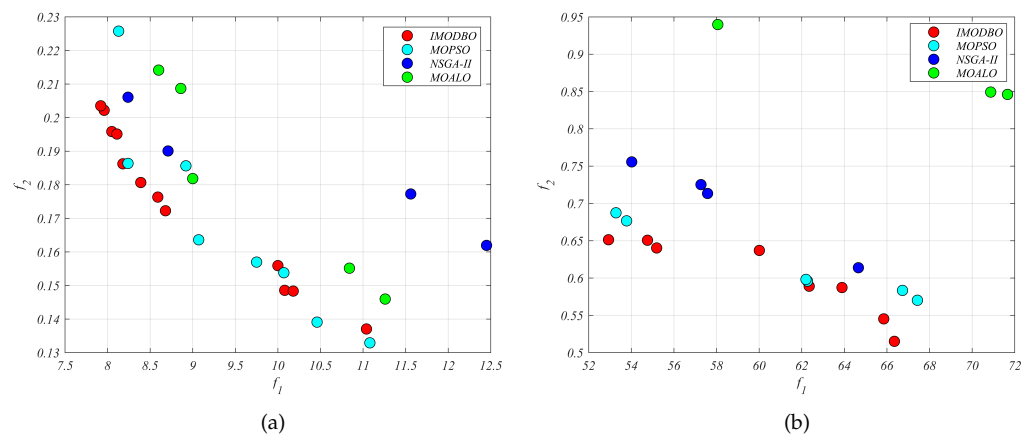


Figure 19. Pareto frontier distribution; (a) IEEE 33-node Pareto front; and (b) PG&E 69-node Pareto front.

Table 10. Multi-objective performance index results.

Algorithm Type	IEEE 33-Node		PG&E 69-Node	
	IGD	HV	IGD	HV
IMODBO	0.0492	0.0895	0.4714	0.0702
MOALO	0.4943	0.0504	3.9928	0
NSGA-II	0.5557	0.0399	1.4131	0.0369
MOPSO	0.1604	0.0824	0.9051	0.0562

In terms of the IGD index, IMODBO demonstrates the lowest value among the four algorithms, indicating its superior convergence and diversity. This signifies that IMODBO is capable of finding solutions that are closer to the true Pareto front. Additionally, the HV index also shows that IMODBO achieves the highest values, outperforming the other algorithms by a significant margin. This confirms the exceptional performance of IMODBO in generating solutions that cover a wide range of objectives. In summary, the multi-objective distribution network dynamic reconfiguration method based on the IMODBO proposed in this paper exhibits significant advantages in terms of convergence and diversity. It showcases superior performance compared to MOALO, NSGA-II, and MOPSO.

5. Conclusions

This study proposes an optimization method based on the improved multi-objective dung beetle optimizer (IMODBO) to address the dynamic reconfiguration optimization problem in distribution networks with distributed power sources. The IMODBO method, in conjunction with the K-means++ clustering algorithm, is proposed and validated for this problem. Furthermore, multiple scenarios are designed in standard distribution network systems to verify the effectiveness of the proposed method. The main contributions of this study are as follows:

- Through testing on both single-objective and multi-objective test functions, the IMODBO algorithm outperforms other optimization algorithms such as DBO, ISSA, NGO, WOA, and GWO in terms of convergence rate, convergence accuracy, and overall performance in single-objective optimization. In multi-objective optimization, the IMODBO algorithm exhibits better performance than MOALO, NSGA-II, MODA, MOSMA, MOPSO, and MOWOA in terms of convergence, solution set distribution, and comprehensive performance.
- An optimization scheme is proposed for dynamic reconfiguration in distribution networks with distributed power sources, utilizing the IMODBO algorithm and K-means++ clustering algorithm. The objective is to reduce the active power loss, stabilize node voltages, and minimize switch operations.
- In the IEEE-33 nodes and PG69 nodes test systems, the proposed method achieves the minimum active power loss and voltage deviation among multiple scenarios. In a single-period comparison experiment, the Pareto solutions obtained by the IMODBO algorithm dominate over the solutions obtained by NSGA-II, MOALO, and MOPSO algorithms. The proposed method also exhibits good performance in terms of multi-objective performance metrics. The Pareto solutions obtained by the IMODBO algorithm have the minimum IGD and maximum HV values in both test systems. This indicates that the proposed method can simultaneously seek solutions that are close to the optimal Pareto front and provide diverse options for decision makers.

This study has significant implications for achieving sustainable energy goals. The proposed IMODBO method demonstrates superior optimization performance and provides an effective solution to reduce energy loss and improve power quality in distribution networks. However, there are limitations to this study. For instance, it does not consider the randomness of photovoltaic power generation and wind power generation. Future research should take into account more factors to make the results more applicable to real-world projects. Additionally, testing in larger and more complex systems with a wider range

of distributed power sources can be conducted to further increase the penetration rate of renewable energy and achieve carbon reduction and neutrality goals.

Author Contributions: Conceptualization, N.T. and Z.F.; methodology, N.T. and Z.F.; software, N.T. and Z.F.; validation, N.T. and Z.F.; formal analysis, Z.F.; investigation, Z.F.; resources, N.T. and Z.F.; data curation, Z.F.; writing—original draft preparation, Z.F.; writing—review and editing, Z.F.; visualization, N.T. and Z.F.; project administration, N.T. and Z.F.; funding acquisition, N.T. All authors have read and agreed to the published version of the manuscript.

Funding: National Natural Science Foundation of China (61601212, 52177047) and Liaoning Provincial Department of Education Fund (LJ2019JL011, LJ2017QL012).

Institutional Review Board Statement: Not applicable.

Informed Consent Statement: Not applicable.

Data Availability Statement: Not applicable.

Conflicts of Interest: The authors declare no conflict of interest.

Nomenclature

DBO	Dung beetle optimizer
DFR	Distribution feeder reconfiguration
DG	Distributed generation
EMA	Exchange market algorithm
GWO	Gray wolf optimizer
HV	Hypervolume
IGD	Inverted generational distance
IMODBO	Improved multi-objective dung beetle optimizer
ISSA	Improved salp swarm algorithm
MODA	Multi-objective dragonfly algorithm
MOPSO	Multi-objective particle swarm optimization
MOSMA	Multi-objective slime mold algorithm
MOALO	Multi-objective ant lion optimizer
MOWOA	Multi-objective whale optimization algorithm
NGO	Northern goshawk optimization
NSGA-II	Non-dominated sorting genetic algorithm II
PSO	Particle swarm optimization
WGA	Wild goats algorithm
WOA	Whale optimization algorithm

Notations

A	Single photovoltaic panel area
B	Conductance
δ	Phase angle difference
F_1	Objective function 1
F_2	Objective function 2
G	Susceptance
$k_{t,l}$	First state at the l -th branch during the t -th period
L_v	Levy flight
N	Total number of nodes in the model
O	Collection dataset
P	Active power (kW)
P_{DG}	DG active power output (kW)
P_{load}	Residential load active power (kW)
P_{PV}	Photovoltaic panel active power (kW)
P_r	Rated active power of the wind turbine (kW)
P_w	Active power of the wind turbine (kW)
pop	Population size
Q	Reactive power (KVar)

Q_{DG}	DG reactive power output (kVar)
Q_{load}	Living load reactive power (kVar)
T	Reconfiguration interval
U	Voltage (kV)
U^*	Rated voltage (kV)
v	Wind speed
W	Adaptive weight factor
η	Conversion efficiency of the battery

References

- Wang, B.; Wang, L.; Zhong, S.; Xiang, N.; Qu, Q. Low-Carbon Transformation of Electric System against Power Shortage in China: Policy Optimization. *Energies* **2022**, *15*, 1574. [\[CrossRef\]](#)
- Zhang, Z.; Hu, G.; Mu, X.; Kong, L. From low carbon to carbon neutrality: A bibliometric analysis of the status, evolution and development trend. *J. Environ. Manag.* **2022**, *322*, 116087. [\[CrossRef\]](#) [\[PubMed\]](#)
- Pang, X.; Zhang, X.; Liu, W.; Li, H.; Wang, Y. Optimal scheduling of cogeneration system with heat storage device based on artificial bee colony algorithm. *Electronics* **2022**, *11*, 1725. [\[CrossRef\]](#)
- Kabeyi, M.J.B.; Olanrewaju, O.A. Sustainable energy transition for renewable and low carbon grid electricity generation and supply. *Front. Energy Res.* **2022**, *9*, 1032. [\[CrossRef\]](#)
- Martí, J.R.; Ahmadi, H.; Bashualdo, L. Linear power-flow formulation based on a voltage-dependent load model. *IEEE Trans. Power Deliv.* **2013**, *28*, 1682–1690. [\[CrossRef\]](#)
- Sarma, N.; Rao, K.P. A new 0–1 integer programming method of feeder reconfiguration for loss minimization in distribution systems. *Electr. Power Syst. Res.* **1995**, *33*, 125–131. [\[CrossRef\]](#)
- Dejamkhooy, A.; Fathi Khaneghah, Y.; Shayeghi, H. Modified branch exchange reconfiguration of active distributed network for simultaneous loss reduction and power quality improvement. *Int. Trans. Electr. Energy Syst.* **2019**, *29*, e12065. [\[CrossRef\]](#)
- Zhan, J.; Liu, W.; Chung, C.; Yang, J. Switch opening and exchange method for stochastic distribution network reconfiguration. *IEEE Trans. Smart Grid* **2020**, *11*, 2995–3007. [\[CrossRef\]](#)
- Sun, Q.; Yu, Y.; Li, D.; Hu, X. A distribution network reconstruction method with DG and EV based on improved gravitation algorithm. *Syst. Sci. Control. Eng.* **2021**, *9*, 6–13. [\[CrossRef\]](#)
- He, Y.; Guo, Y. Fault Reconstruction of Medium Voltage DC Power System in Ships Based on Simulated Annealing Particle Swarm Algorithm. In Proceedings of the 2022 4th International Conference on Electrical Engineering and Control Technologies (CEECT), Shanghai, China, 16–18 December 2022; IEEE: Piscataway, NJ, USA, 2022; pp. 140–144.
- Li, L.L.; Liu, Z.F.; Tseng, M.L.; Zheng, S.J.; Lim, M.K. Improved tunicate swarm algorithm: Solving the dynamic economic emission dispatch problems. *Appl. Soft Comput.* **2021**, *108*, 107504. [\[CrossRef\]](#)
- Li, L.L.; Xiong, J.L.; Tseng, M.L.; Yan, Z.; Lim, M.K. Using multi-objective sparrow search algorithm to establish active distribution network dynamic reconfiguration integrated optimization. *Expert Syst. Appl.* **2022**, *193*, 116445. [\[CrossRef\]](#)
- Wang, H.J.; Pan, J.S.; Nguyen, T.T.; Weng, S. Distribution network reconfiguration with distributed generation based on parallel slime mould algorithm. *Energy* **2022**, *244*, 123011. [\[CrossRef\]](#)
- Gao, J.; Gao, F.; Ma, Z.; Huang, N.; Yang, Y. Multi-objective optimization of smart community integrated energy considering the utility of decision makers based on the Lévy flight improved chicken swarm algorithm. *Sustain. Cities Soc.* **2021**, *72*, 103075. [\[CrossRef\]](#)
- Mahdad, B. Optimal reconfiguration and reactive power planning based fractal search algorithm: A case study of the Algerian distribution electrical system. *Eng. Sci. Technol. Int. J.* **2019**, *22*, 78–101. [\[CrossRef\]](#)
- Kefayat, M.; Ara, A.L.; Niaki, S.N. A hybrid of ant colony optimization and artificial bee colony algorithm for probabilistic optimal placement and sizing of distributed energy resources. *Energy Convers. Manag.* **2015**, *92*, 149–161. [\[CrossRef\]](#)
- Jafari, A.; Ganjehlou, H.G.; Darbandi, F.B.; Mohammadi-Ivatloo, B.; Abapour, M. Dynamic and multi-objective reconfiguration of distribution network using a novel hybrid algorithm with parallel processing capability. *Appl. Soft Comput.* **2020**, *90*, 106146. [\[CrossRef\]](#)
- Parizad, A.; Baghaee, H.; Yazdani, A.; Gharehpetian, G. Optimal distribution systems reconfiguration for short circuit level reduction using PSO algorithm. In Proceedings of the 2018 IEEE Power and Energy Conference at Illinois (PECI), Champaign, IL, USA, 22–23 February 2018; IEEE: Piscataway, NJ, USA, 2018; pp. 1–6.
- Xue, J.; Shen, B. Dung beetle optimizer: A new meta-heuristic algorithm for global optimization. *J. Supercomput.* **2022**, *79*, 7305–7336. [\[CrossRef\]](#)
- Nguyen, T.T.; Nguyen, T.T.; Duong, L.T.; Truong, V.A. An effective method to solve the problem of electric distribution network reconfiguration considering distributed generations for energy loss reduction. *Neural Comput. Appl.* **2021**, *33*, 1625–1641. [\[CrossRef\]](#)

21. Salkuti, S.R. Network Reconfiguration of Distribution System with Distributed Generation, Shunt Capacitors and Electric Vehicle Charging Stations. In *Next Generation Smart Grids: Modeling, Control and Optimization*; Springer: Berlin/Heidelberg, Germany, 2022; pp. 355–375.
22. Pegado, R.; Naupari, Z.; Molina, Y.; Castillo, C. Radial distribution network reconfiguration for power losses reduction based on improved selective BPSO. *Electr. Power Syst. Res.* **2019**, *169*, 206–213. [[CrossRef](#)]
23. Wang, J.; Wang, W.; Yuan, Z.; Wang, H.; Wu, J. A chaos disturbed beetle antennae search algorithm for a multiobjective distribution network reconfiguration considering the variation of load and DG. *IEEE Access* **2020**, *8*, 97392–97407. [[CrossRef](#)]
24. Tran, T.T.; Truong, K.H.; Vo, D.N. Stochastic fractal search algorithm for reconfiguration of distribution networks with distributed generations. *Ain Shams Eng. J.* **2020**, *11*, 389–407. [[CrossRef](#)]
25. Amin, A.; Tareen, W.U.K.; Usman, M.; Memon, K.A.; Horan, B.; Mahmood, A.; Mekhilef, S. An integrated approach to optimal charging scheduling of electric vehicles integrated with improved medium-voltage network reconfiguration for power loss minimization. *Sustainability* **2020**, *12*, 9211. [[CrossRef](#)]
26. George, D.T.; Raj, R.E.; Rajkumar, A.; Mabel, M.C. Optimal sizing of solar-wind based hybrid energy system using modified dragonfly algorithm for an institution. *Energy Convers. Manag.* **2023**, *283*, 116938. [[CrossRef](#)]
27. Fares, D.; Fathi, M.; Mekhilef, S. Performance evaluation of metaheuristic techniques for optimal sizing of a stand-alone hybrid PV/wind/battery system. *Appl. Energy* **2022**, *305*, 117823. [[CrossRef](#)]
28. Lu, Q.; Wang, X.; Xiao, J. Dynamic reconfiguration of distribution network with distributed power supply based on improved artificial fish-swarm algorithm. In Proceedings of the 2022 4th International Academic Exchange Conference on Science and Technology Innovation (IAECST), Guangzhou, China, 9–11 December 2022; pp. 210–215.
29. Wang, X.; Liu, X.; Jian, S.; Peng, X.; Yuan, H. A distribution network reconfiguration method based on comprehensive analysis of operation scenarios in the long-term time period. *Energy Rep.* **2021**, *7*, 369–379. [[CrossRef](#)]
30. Li, Y.; Han, M.; Guo, Q. Modified whale optimization algorithm based on tent chaotic mapping and its application in structural optimization. *KSCE J. Civ. Eng.* **2020**, *24*, 3703–3713. [[CrossRef](#)]
31. Wu, J.; Nan, R.; Chen, L. Improved salp swarm algorithm based on weight factor and adaptive mutation. *J. Exp. Theor. Artif. Intell.* **2019**, *31*, 493–515. [[CrossRef](#)]
32. Li, J.; An, Q.; Lei, H.; Deng, Q.; Wang, G.G. Survey of lévy flight-based metaheuristics for optimization. *Mathematics* **2022**, *10*, 2785. [[CrossRef](#)]
33. Ouyang, C.; Qiu, Y.; Zhu, D. Adaptive spiral flying sparrow search algorithm. *Sci. Program.* **2021**, *2021*, 6505253. [[CrossRef](#)]
34. Gharehchopogh, F.S.; Gholizadeh, H. A comprehensive survey: Whale Optimization Algorithm and its applications. *Swarm Evol. Comput.* **2019**, *48*, 1–24. [[CrossRef](#)]
35. Mirjalili, S.; Mirjalili, S.M.; Lewis, A. Grey wolf optimizer. *Adv. Eng. Softw.* **2014**, *69*, 46–61. [[CrossRef](#)]
36. Dehghani, M.; Hubálovský, Š.; Trojovský, P. Northern goshawk optimization: A new swarm-based algorithm for solving optimization problems. *IEEE Access* **2021**, *9*, 162059–162080. [[CrossRef](#)]
37. Ibrahim, R.A.; Ewees, A.A.; Oliva, D.; Abd Elaziz, M.; Lu, S. Improved salp swarm algorithm based on particle swarm optimization for feature selection. *J. Ambient. Intell. Humaniz. Comput.* **2019**, *10*, 3155–3169. [[CrossRef](#)]
38. Deb, K.; Pratap, A.; Agarwal, S.; Meyarivan, T. A fast and elitist multiobjective genetic algorithm: NSGA-II. *IEEE Trans. Evol. Comput.* **2002**, *6*, 182–197. [[CrossRef](#)]
39. Mirjalili, S.; Jangir, P.; Saremi, S. Multi-objective ant lion optimizer: A multi-objective optimization algorithm for solving engineering problems. *Appl. Intell.* **2017**, *46*, 79–95. [[CrossRef](#)]
40. Joshi, M.; Ghadai, R.K.; Madhu, S.; Kalita, K.; Gao, X.Z. Comparison of NSGA-II, MOALO and MODA for multi-objective optimization of micro-machining processes. *Materials* **2021**, *14*, 5109. [[CrossRef](#)]
41. Premkumar, M.; Jangir, P.; Sowmya, R.; Alhelou, H.H.; Heidari, A.A.; Chen, H. MOSMA: Multi-objective slime mould algorithm based on elitist non-dominated sorting. *IEEE Access* **2020**, *9*, 3229–3248. [[CrossRef](#)]
42. Baghaee, H.R.; Mirsalim, M.; Gharehpetian, G.B.; Kaviani, A.K. Security/cost-based optimal allocation of multi-type FACTS devices using multi-objective particle swarm optimization. *Simulation* **2012**, *88*, 999–1010. [[CrossRef](#)]
43. Baghaee, H.R.; Mirsalim, M.; Gharehpetian, G.B.; Talebi, H.A. MOPSO/FDMT-based Pareto-optimal solution for coordination of overcurrent relays in interconnected networks and multi-DER microgrids. *IET Gener. Transm. Distrib.* **2018**, *12*, 2871–2886. [[CrossRef](#)]
44. Kumawat, I.R.; Nanda, S.J.; Maddila, R.K. Multi-objective whale optimization. In Proceedings of the Tencon 2017–2017 IEEE Region 10 Conference, Penang, Malaysia, 5–8 November 2017; IEEE: Piscataway, NJ, USA, 2017; pp. 2747–2752.
45. Jiang, S.; Yang, S. An improved multiobjective optimization evolutionary algorithm based on decomposition for complex Pareto fronts. *IEEE Trans. Cybern.* **2015**, *46*, 421–437. [[CrossRef](#)]
46. Sandoval, C.; Cuate, O.; González, L.C.; Trujillo, L.; Schütze, O. Towards fast approximations for the hypervolume indicator for multi-objective optimization problems by Genetic Programming. *Appl. Soft Comput.* **2022**, *125*, 109103. [[CrossRef](#)]
47. Li, M.; Yang, S.; Liu, X. Pareto or non-Pareto: Bi-criterion evolution in multiobjective optimization. *IEEE Trans. Evol. Comput.* **2015**, *20*, 645–665. [[CrossRef](#)]

48. Baran, M.E.; Wu, F.F. Network reconfiguration in distribution systems for loss reduction and load balancing. *IEEE Trans. Power Deliv.* **1989**, *4*, 1401–1407. [[CrossRef](#)]
49. Savier, J.; Das, D. Impact of network reconfiguration on loss allocation of radial distribution systems. *IEEE Trans. Power Deliv.* **2007**, *22*, 2473–2480. [[CrossRef](#)]

Disclaimer/Publisher’s Note: The statements, opinions and data contained in all publications are solely those of the individual author(s) and contributor(s) and not of MDPI and/or the editor(s). MDPI and/or the editor(s) disclaim responsibility for any injury to people or property resulting from any ideas, methods, instructions or products referred to in the content.